Defense Technical Information Center
Compilation Part Notice

ADP011210

TITLE: The Role of Electrode Microstructure on Activation and Concentration Polarizations in Solid Oxide Fuel Cells

DISTRIBUTION: Approved for public release, distribution unlimited

This paper is part of the following report:

TITLE: Internal Workshop on Interfacially Controlled Functional Materials: Electrical and Chemical Properties Held in Schloss Ringberg, Germany on March 8-13, 1998

To order the complete compilation report, use: ADA397655

The component part is provided here to allow users access to individually authored sections of proceedings, annals, symposia, etc. However, the component should be considered within the context of the overall compilation report and not as a stand-alone technical report.

The following component part numbers comprise the compilation report:
ADP011194 thru ADP011211

The role of electrode microstructure on activation and concentration polarizations in solid oxide fuel cells[☆]

Anil V. Virkar[*], Jong Chen, Cameron W. Tanner, Jai-Woh Kim

University of Utah, Department of Materials Science & Engineering, 304 EMRO, 122 S. Central Campus Drive, Salt Lake City, UT 84112, USA

Abstract

Activation and concentration polarization effects in anode-supported solid oxide fuel cells (SOFC) were examined. The anode and the cathode consisted respectively of porous, composite, contiguous mixtures of Ni + yttria-stabilized zirconia (YSZ) and Sr-doped $LaMnO_3$ (LSM) + YSZ. The composite electrode provides parallel paths for oxygen ions (through YSZ), electrons (through the electronic conductor; Ni for the anode and LSM for the cathode), and gaseous species (through the pores) and thereby substantially decreases the activation polarization. The composite electrode effectively spreads the charge transfer reaction from the electrolyte/electrode interface into the electrode. At low current densities where the activation polarization can be approximated as being ohmic, an effective charge transfer resistance, R_{ct}^{eff}, is defined in terms of various parameters, including the intrinsic charge transfer resistance, R_{ct}, which is a characteristic of the electrocatalyst/electrolyte pair (e.g. LSM/YSZ), and the electrode thickness. It is shown that the R_{ct}^{eff} attains an asymptotic value at large electrode thicknesses. The limiting value of R_{ct}^{eff} can be either lower or higher than R_{ct} depending upon the magnitudes of the ionic conductivity, σ_i, of the composite electrode, the intrinsic charge transfer resistance, R_{ct}, and the grain size of the electrode. For an R_{ct} of 1.2 Ωcm^2, σ_i of 0.02 S/cm and an electrode grain size of 2 μm, the limiting value of R_{ct}^{eff} is 0.14 Ωcm^2 indicating almost an order of magnitude decrease in activation polarization. The experimental measurements on the cell resistance of anode-supported cells as a function of the cathode thickness are in accord with the theoretical model. The concentration polarization is analyzed by taking into account gas transport through porous electrodes. It is shown that the voltage, V, vs. current density, i, traces should be nonlinear and in anode-supported cells, the initial concave up curvature ($d^2V/di^2 \geq 0$) has its origin in both activation and concentration polarizations. The experimental results are consistent with the theoretical model. © 2000 Elsevier Science B.V. All rights reserved.

Keywords: Electrode microstructure; Activation; Concentration polarization; Solid oxide; Fuel cell

1. Introduction

Solid state devices such as solid oxide fuel cells (SOFC) consist of a cathode, an electrolyte, and an anode. Two basic designs have been explored in the development of the SOFC; the electrolyte-supported

and the electrode-supported [1]. In the former, the electrolyte is the thickest component and is effectively the support structure. In electrolyte-supported cells, the thickness of the electrolyte, typically YSZ, is ≥ 150 μm with thin electrodes screen-printed on it [2,3]. In the latter, one of the two electrodes, either the cathode or the anode, is the thickest component and the support structure.

In electrolyte-supported cells the ohmic contribution is large due to high electrolyte resistivity. For this reason, such cells are being developed for operation at $\sim 1000°C$ where the electrolyte resistivity is low, typically ~ 20 Ωcm. In cathode-supported cells, a 30–40 μm layer of YSZ is deposited on a porous LSM cathode of ~ 2 mm thickness [4]. Similarly, in anode-supported cells, a YSZ layer of 10–20 μm thickness is deposited on a relatively thick Ni + YSZ anode [1,5].

The overall performance of such devices is dictated by various polarizations; namely ohmic, activation, and concentration. The main contribution to the ohmic polarization is due to the electrolyte. A high ionic conductivity and a small electrolyte thickness are the desired characteristics of the solid electrolyte to minimize the ohmic contribution. Although various solid electrolytes with high ionic conductivities at moderate temperatures have been explored, yttria-stabilized zirconia (YSZ) is by far the most widely used solid electrolyte due to its excellent stability in both reducing and oxidizing environments, even though its conductivity is lower (resistivity is higher) than other materials such as ceria and Sr- and Mg-doped $LaGaO_3$ (LSGM). In electrolyte-supported cells, the typical YSZ membrane thickness is 150 μm. At 800°C, the resistivity of YSZ is about 50 Ωcm which translates into an area specific resistance (electrolyte contribution) of about 0.75 $Ωcm^2$. This value is very high with the result that the power density is rather low at temperatures below about 950°C. However, in electrode-supported cells, the YSZ electrolyte thickness need only be about 10 μm. With a 10 μm thick YSZ film as the electrolyte, the area specific resistance of the electrolyte is only about 0.05 $Ωcm^2$ at 800°C thus making an efficient operation of an SOFC at such a low temperature in principle possible. However, it is usually observed that despite a low ohmic contribution, the area

specific resistance of the cell as a whole may be several times larger. The reason is that activation and concentration polarizations can often outweigh the ohmic contribution. Thus, the minimization of the overall area specific resistance of cells requires an optimization of parameters which govern the activation and concentration polarization effects.

Activation polarization is related to charge transfer processes and thus depends upon the nature of electrode–electrolyte interfaces. In composite electrodes comprising a mixture of an ionic conductor and an electronic conductor, or in a single phase mixed ionic electronically conducting (MIEC) electrode, the process of charge transfer is expected to occur over some distance from the electrolyte/electrode interface into the electrode. That is, effectively the interface is diffuse insofar as the region over which charge transfer occurs. Concentration polarization is related to the transport of gaseous species through porous electrodes, and thus is related to the microstructure of the electrodes; specifically the volume percent porosity, the pore size, and the tortuosity factor. It is thus clear that a reduction in the overall area specific resistance of cells and a concomitant improvement in cell performance can be achieved only through a reduction in these two polarization effects. Indeed, recent work has shown that an area specific resistance less than 0.15 $Ωcm^2$ can be realized in anode-supported cells at 800°C with a maximum power density in excess of 1.8 $Ω/cm^2$ [6]. This was achieved by minimizing both activation and concentration polarizations. Effectively, the microstructures of the electrodes and the electrolyte/electrode interfaces were tailored to minimize these polarization effects. In this paper, these two polarization effects are examined in light of anode-supported SOFCs.

2. Activation polarization

The role of composite electrodes, comprising a mixture of a solid electrolyte and an electronic conductor, or a mixed ionic–electronically conducting (MIEC) material, on electrode kinetics has been examined by a number of researchers [7–11]. The rationale for the use of a composite or an MIEC

electrode is that it allows a spreading of the reaction zone from the electrolyte/electrode interface into the electrode. That is, effectively it results in a sort of a diffuse electrolyte/electrode interface wherein the charge transfer reaction occurs. Even though it has been proposed by some that in a mixed conducting material as an electrode the charge transfer reaction can occur over the entire surface, it is generally thought to occur at electrolyte–electrocatalyst–gas three phase boundaries (TPB), which are also high energy sites. In a single phase MIEC electrode, the charge transfer may predominantly occur at high energy sites such as grain boundaries and defects in the MIEC at the MIEC/gas phase interface. Tanner et al. [11] examined charge transfer reactions in a composite electrode. For the case of SOFC, for example, the analysis is applicable to Ni+YSZ anode and to LSM+YSZ cathode. It is known that the electrode overpotential at a Ni+YSZ electrode is usually negligible and much of the activation polarization can be attributed to the cathode. In this context, the following discussion is particularly applicable to Sr-doped LaMnO$_3$ (LSM)+YSZ cathode. The electrocatalytic properties of LSM over YSZ can in principle be described in terms of a phenomenological model such as the Butler–Volmer equation which relates the current density, i, to the activation overpotential, η_{act}, by

$$i = i_o \left\{ \exp\left(\frac{\alpha z F \eta_{act}}{RT}\right) - \exp\left(\frac{-(1-\alpha)z F \eta_{act}}{RT}\right) \right\} \tag{1}$$

where i_o is the exchange current density, α is the transfer coefficient, z is the number of electrons participating in the electrode reaction, F is the Faraday constant, R is the gas constant, and T is the temperature. In the low current density regime,

$$\eta_{act} \approx \frac{RT}{zFi_o} i = R_{ct} i \tag{2}$$

where R_{ct} given by

$$R_{ct} = \frac{RT}{zFi_o} \tag{3}$$

is the intrinsic charge transfer resistance in Ωcm^2. It is a function of the electrochemical properties of the electrocatalyst/electrolyte pair (LSM/YSZ here), and also a function of the TPB line length. Thus, it is a function of the particle size of LSM and the amount of LSM per unit area of YSZ. In what follows, R_{ct} will be treated as an empirical parameter, determined experimentally for a given electrocatalyst/electrolyte pair. In composite electrodes comprising a mixture of LSM+YSZ for instance, the reaction zone, that is the region over which the process of charge transfer occurs, is spread out from the electrolyte/electrode interface into the electrode. In such a case, it is expected that the activation overpotential, η_{act}, may be lower than that given by Eq. (2). Tanner et al. [11] defined an effective charge transfer resistance, R_{ct}^{eff}, given by

$$\eta_{act} \approx R_{ct}^{eff} i \tag{4}$$

Using this as a parameter for the design of composite electrodes, Tanner et al. [11] derived an expression for R_{ct}^{eff} terms of R_{ct} and the ionic conductivity of the electrode, σ_i, which describe the properties of the electrode/electrolyte interface and the electrolyte, respectively, and microstructural parameters of the electrode, namely the grain size and porosity. This equation is given by [11]

$$R_{ct}^{eff} = \frac{BR_{ct}}{B\left(\dfrac{1+\beta}{1+\beta\exp\left(-\dfrac{2h}{\lambda}\right)}\right)(1-V_\nu)\exp\left(-\dfrac{h}{\lambda}\right) + \left(\dfrac{1+\beta\exp\left(-\dfrac{h}{\lambda}\right)}{1+\beta\exp\left(-\dfrac{2h}{\lambda}\right)}\right)\lambda\left(1-\exp\left(-\dfrac{h}{\lambda}\right)\right) + bV_\nu} \tag{5}$$

where

$$\lambda = \sqrt{\sigma_i B(1 - V_\nu)R_{ct}} \quad \text{and} \quad \beta = \frac{\sigma_i R_{ct} - \lambda}{\sigma_i R_{ct} + \lambda} \quad (6)$$

in which B is the grain size of the electrolyte in the composite electrode, V_ν denotes the fractional porosity, and h is the electrode thickness. It is to be emphasized that the ionic conductivity of the electrode, σ_i in general may be different from that of the dense electrolyte membrane. For example, the electrolyte membrane may be of say YSZ but the electrode may contain doped ceria. The analysis assumes that the electronic conductivity of the electrode is much larger than the ionic conductivity, and gas transport through the electrode is not rate-limiting. Eq. (5) shows that the effective charge transfer resistance, R_{ct}^{eff} approaches R_{ct} as $h \to 0$, and achieves an asymptotic value with an increasing electrode thickness. It can be shown that as $h \to \infty$, the R_{ct}^{eff} is given by [11]

$$R_{ct}^{eff} \approx \sqrt{\frac{BR_{ct}}{\sigma_i(1 - V_\nu)}} \quad (7)$$

as long as σ_i is not too small. As $\sigma_i \to 0$, the asymptotic value of R_{ct}^{eff} is given by

$$R_{ct}^{eff} \approx \frac{R_{ct}}{V_\nu} \quad (8)$$

If $\sigma_i \to 0$, it means that only the three phase boundary (TPB) at the surface of the electrocatalyst/dense electrolyte membrane (e.g. LSM and the dense YSZ membrane) contributes to the charge transfer reaction; hence the presence of V_ν in the denominator of Eq. (8). Eqs. (6) and (7) also show the effect of the microstructural dimension, B, which is essentially the grain size of YSZ in the electrode. As an illustration, let us choose the following values: $R_{ct} = 1.2 \ \Omega\text{cm}^2$, $\sigma_i = 0.02 \ \text{S/cm}$, $B = 2 \ \mu\text{m}$, and $= V_\nu = 0.35$. Then, the estimated value of the effective charge transfer resistance R_{ct}^{eff} is 0.14 Ωcm^2, almost an order of magnitude decrease in the charge transfer resistance, or an order of magnitude increase in the effective exchange current density, $i_{o(eff)}$. This shows the profound effect of composite, mixed conducting electrodes on electrode kinetics.

Eq. (7) shows that the effect of composite electrode need not always be an enhancement in electrode kinetics. Indeed, Eq. (7) shows that

$$R_{ct}^{eff} \leq R_{ct} \quad \text{if} \quad \frac{B}{\sigma_i(1 - V_\nu)} \leq R_{ct}$$

However,

$$\frac{R_{ct}}{V_\nu} \geq R_{ct}^{eff} \geq R_{ct} \quad \text{if} \quad \frac{B}{\sigma_i(1 - V_\nu)} \geq R_{ct}$$

That is, the electrode kinetics could actually be suppressed if the electrode parameters are unfavorable; e.g. too coarse a microstructure (large B) and/or too low an ionic conductivity, σ_i, of the electrolyte material in the electrode (or too low an ionic conductivity of a single phase MIEC electrode). As an example, a suppression of the electrode kinetics would occur if an SOFC anode is made of Ni + an inert material, such as α-alumina. Since α-alumina is not an oxygen ion conductor, its σ_i is essentially zero. In such a case, the electrode polarization should actually increase when using such a composite electrode. Fig. 1 shows plots of R_{ct}^{eff} vs. log h (Eq. (5)) for various values of σ_i. Note that the R_{ct}^{eff} can either decrease or increase depending upon the value of σ_i for given values of R_{ct}, B and V_ν. The experimental results of Kenjo et al. [7] on composite electrodes showed that in some cases, the polarization resistance decreased with an increasing electrode thickness, while in other cases there appeared to be no effect of the thickness. These observations are at variance with the predictions of the model by Kenjo et al. [7]. However, their results are entirely consistent with the model presented by Tanner et al. [11].

Eq. (5) shows the dependence of R_{ct}^{eff} on h. For values of h greater than the critical value, R_{ct}^{eff} achieves an asymptotic value given by Eq. (7). An experimental verification of the dependence of the asymptotic value of R_{ct}^{eff} on electrode thickness was obtained on anode-supported solid oxide fuel cells with a varying cathode thickness. The anode (Ni + YSZ) thickness was typically 1 mm with an electrolyte (YSZ) thickness of ~20 μm. The cathode thickness was varied over a range between ~0 to ~85 μm. The cathode was prepared by first forming a porous layer of YSZ on the dense YSZ electrolyte layer, and then infiltrating an aqueous solution of
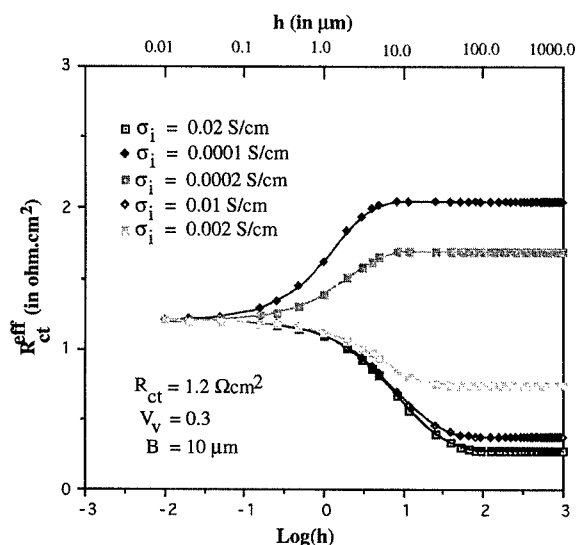
Fig. 1. Theoretically calculated values of the effective charge transfer resistance, R_{ct}^{eff}, for an intrinsic charge transfer resistance, R_{ct}, of 1.2 Ωcm^2 for several values of the ionic conductivity, σ_i, of the composite electrode. At high values of σ_i, the R_{ct}^{eff} decreases with an increasing electrode thickness, h, and achieves a limiting value. However, it is seen that for low values of σ_i, the R_{ct}^{eff} actually increases with the electrode thickness, h. That is, under such conditions, the composite electrode may actually suppress electrode kinetics (enhance electrode polarization).

La-nitrate, Sr-nitrate, and Mn-nitrate. After salt infiltration, the cells were heated to 1000°C to decompose the salts and form LSM. The voltage, V, vs. current density, i, performance curves were measured at 800°C with humidified hydrogen as the fuel and air as the oxidant. Fig. 2 shows the voltage vs. current density polarization curves for a number of cells for different cathode thicknesses. It is clearly seen that the performance increases with an increasing cathode thickness up to ~45 μm. For the cell with a cathode thickness of ~85 μm, the performance is somewhat lower than for the cell with a ~45 μm cathode. This is attributed to three possible reasons: (a) The method of deposition of the porous YSZ layer of the cathode was not optimized which led to a highly tortuous path for the transport of gaseous species. This presumably led to a significant concentration polarization, especially at larger cathode thicknesses. (b) In this nonoptimized method for the preparation of the cathode layer, some cracking of the layer with cracks parallel to the
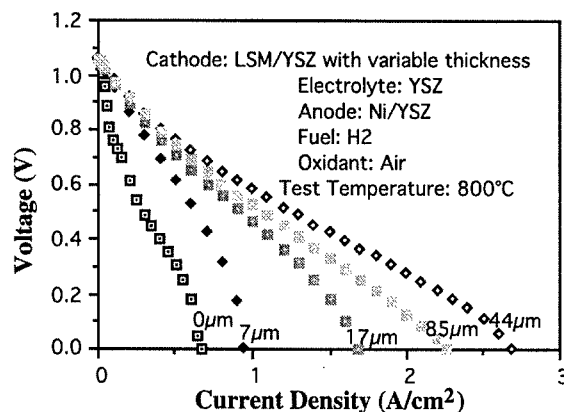

Fig. 2. The experimentally measured voltage, V, vs. current density, i, traces for anode-supported cells with varying cathode thicknesses. Note that, in general, the performance increases with an increase in cathode thickness.

electrolyte/cathode interface is possible. This may have led to some increase in the resistance. (c) The method of introducing the salt solutions was not optimized which may have led to a nonuniform distribution of the subsequent LSM formed after calcination. It is nevertheless clear that the cell performance indeed increases with an increasing cathode thickness. From the near linear regions of the voltage vs. current density traces, the cell resistance was measured. From this, the electrolyte area specific resistance, R_i, calculated using independently measured σ_i and the electrolyte thickness, was subtracted. Neglecting concentration polarization, this gives an approximate estimate of the effective charge transfer resistance, R_{ct}^{eff}. Fig. 3 shows the estimated (experimental) R_{ct}^{eff} vs. the cathode thickness (on a log scale). Also shown is a plot of R_{ct}^{eff} calculated using Eq. (5) with $R_{ct} = 1.2$ Ωcm^2, $\sigma_i = 0.02$ S/cm, $B = 5$ μm, and $V_{\nu} = 0.3$. Note that the agreement between the experimental data and the model is good.

The preceding discussion assumes the activation polarization to be ohmic; i.e. η_{act} being linearly proportional to the current density, i, which is applicable for current densities less than the exchange current density, i_o. The composite electrode thus increases the exchange current density, which may be termed the effective exchange current density, $i_{o(eff)}$, given by
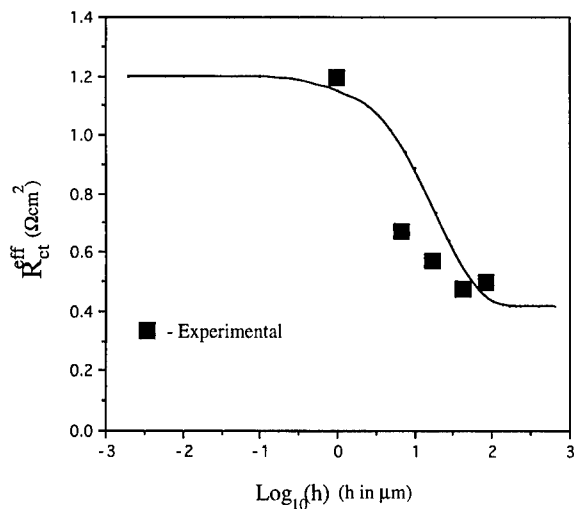
Fig. 3. A plot of R_{ct}^{eff} vs. cathode thickness, h (log scale), calculated using $R_{ct} = 1.2$ Ωcm^2, $\sigma_i = 0.02$ S/cm, and the grain size of YSZ in the cathode $= 5$ μm. Also plotted are the experimentally estimated (approximate, because the V vs. i traces are nonlinear) R_{ct}^{eff} from the data in Fig. 2. The data point corresponding to zero cathode thickness is that corresponding to the LSM paste directly applied on the dense YSZ layer, without a porous YSZ layer. Since the data point corresponding to zero cathode thickness actually represents that for a small but a nonzero thickness, and that zero thickness can not be shown on a log scale, this data point is shown at $h = 1$ μm.

$$i_{o(eff)} \approx \frac{RT}{zFR_{ct}^{eff}} \qquad (9)$$

However, at large current densities, either the Butler–Volmer or the Tafel equation will be applicable. Preliminary calculations have shown that the composite electrode can be effective in decreasing the η_{act} in a similar manner, although an explicit analytical form is not available. In the Tafel limit, the η_{act} may be given by

$$\eta_{act} \approx a + b \ln i \qquad (10)$$

where the parameters a and b are influenced by the electrode microstructure and the thickness. In what follows, it will be assumed that the activation polarization is adequately described by the Tafel equation and it will be incorporated into the analysis

of the voltage vs. current density traces of cells. Thus, it is tacitly assumed that the composite electrode modifies a and b such that $i_{o(eff)}$ is much larger than i_o.

3. Concentration polarization

Fig. 4 shows schematics of cathode-supported and anode-supported cells. In the former, the cathode is the thickest component of the cell and in the latter the anode is the thickest component. Fig. 4 also shows schematic variations of the partial pressures of the various gaseous species. The analysis of concentration polarization thus should begin with the analysis of the transport of gases through porous electrodes. In the anode, the principal gaseous species are H_2 and H_2O, and in the cathode they are O_2 and N_2. The basic equations describing an isothermal transport of gaseous species through porous electrodes for a mixture of two gases, A and B, are given by [12,13]

$$J_A = -D_A \nabla n_A + X_A \delta_A J - X_A \gamma_A \left(\frac{nB_o}{\mu} \right) \nabla p \qquad (11)$$

$$J_B = -D_B \nabla n_B + X_B \delta_B J - X_B \gamma_B \left(\frac{nB_o}{\mu} \right) \nabla p \qquad (12)$$
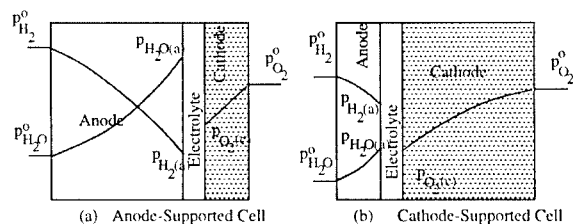
where

(a) Anode-Supported Cell   (b) Cathode-Supported Cell

Fig. 4. Schematics showing the variation of partial pressures of hydrogen, p_{H_2}, and water vapor, p_{H_2O}, through the anode, and oxygen, p_{O_2}, through the cathode of: (a) an anode-supported cell, and (b) a cathode-supported cell.

$$\frac{1}{D_A} = \frac{1}{D_{AK(eff)}} + \frac{1}{D_{AB(eff)}}$$

$$\delta_A = \frac{D_{AK(eff)}}{D_{AK(eff)} + D_{AB(eff)}} \qquad \gamma_A = \frac{D_{B(eff)}}{D_{AK(eff)} + D_{AB(eff)}}$$

$$\frac{1}{D_B} = \frac{1}{D_{BK(eff)}} + \frac{1}{D_{AB(eff)}}$$

$$\delta_B = \frac{D_{BK(eff)}}{D_{BK(eff)} + D_{AB(eff)}} \qquad \gamma_B$$

$$= \frac{D_{AB(eff)}}{D_{BK(eff)} + D_{AB(eff)}} \qquad (13)$$

In Eqs. (11) and (12), the fluxes of A and B are given by J_A and J_B, respectively, $D_{AB(eff)}$ is the effective binary diffusivity (taking into account the porosity and the tortuosity factor), $D_{AK(eff)}$ & $D_{BK(eff)}$ are the effective Knudsen diffusivities, n_A & n_B are the concentrations of A & B (#/cm^3), respectively, $n = (n_A + n_B)$, X_A & X_B are the mole fractions, B_o is the permeability through the porous electrode, μ is the viscosity, p is the total pressure, and J is the total flux. The effective diffusivities are given by the intrinsic diffusivities multiplied by the porosity, V_v, and divided by the tortuosity factor, τ [12–14]. The parameters δ_A & δ_B, and γ_A & γ_B are as defined above. Eqs. (11) and (12) include two flux contributions; a diffusive flux and a viscous flux. The diffusive contribution consists of two terms; a free molecule or Knudsen flow (the terms containing $D_{AK(eff)}$ & $D_{BK(eff)}$), and a continuum part (the terms containing the effective binary diffusivities). The typical total pressure on the anodic and the cathodic sides is on the order of 1 atm or greater, and the typical pore size is ≥ 1 μm. Thus, in general it may be assumed that $D_{AK(eff)}$ & $D_{BK(eff)} \gg D_{AB(eff)}$. Thus, it will be assumed that D_A & D_B can be replaced by $D_{AB(eff)}$ [12]. That is, at high pressures, such as those of interest here, both D_A & D_B approach $D_{AB(eff)}$, the effective binary diffusion coefficient, and δ_A & $\delta_B \rightarrow 1$, and γ_A & $\gamma_B \rightarrow 0$. For the cathode, the D_{AB} is the binary diffusion coefficient for a mixture of oxygen, O_2, and nitrogen, N_2. For the anode, the binary diffusion coefficient is that for H_2 and H_2O. At room temperature, $D_{O_2-N_2} \approx 0.22$ cm^2/s and $D_{H_2-H_2O} \approx 0.91$ cm^2/s [13]. If the fuel also contains CO and CO_2, then their transport

must also be accounted for. The dependence of diffusion coefficient on temperature is not very strong and to a first approximation it may be modified using the kinetic theory of gases. This suggests that for comparable porosities and electrode thicknesses, the concentration polarization effects in general should be less on the anode side.

If the electrode porosity and microstructure are functions of position, and/or $D_{B(eff)}$ is composition-dependent, the variation of partial pressures of the various species with position will not be linear. For this reason, the schematics given in Fig. 4 show nonlinear variations of partial pressures.

In a steady state, the equality

$$|j_{H_2}| = |j_{H_2O}| = 2|j_{O_2}| = \frac{iN_A}{2F} \qquad (14)$$

must hold, where j_{H_2}, j_{H_2O} and j_{O_2} are respectively the fluxes of hydrogen through the porous anode, of water vapor through the porous anode and of oxygen through the porous cathode, and N_A is the Avogadro number. The flux equations were solved for the steady state, subject to the above flux equality requirement [6]. By incorporating the activation polarization (using the Tafel equation) and the concentration polarization (by solving the flux equations for transport through porous electrodes), it was shown that the voltage vs. current density behavior can be adequately described by [6]

$$V(i) = E_o - iR_i - a - b \ln i + \frac{RT}{4F} \ln \left(1 - \frac{i}{i_{cs}} \right)$$

$$+ \frac{RT}{2F} \ln \left(1 - \frac{i}{i_{as}} \right) - \frac{RT}{2F} \ln \left(1 + \frac{p_{H_2}^i i}{p_{H_2O}^o i_{as}} \right) \qquad (15)$$

where E_o is the open circuit voltage (V), R_i is the area specific resistance (ohmic) of the cell (Ωcm^2), $p_{H_2}^o$ is the partial pressure of hydrogen in the fuel (outside of the anode), $p_{H_2O}^o$ is the partial pressure of water vapor in the fuel (outside of the anode), i_{as} is the anode-limiting current density (a current density at which the partial pressure of hydrogen at the anode/electrolyte interface is nearly zero), Amp/cm^2, and i_{cs} is the cathode-limiting current density (a current density at which the partial pressure of
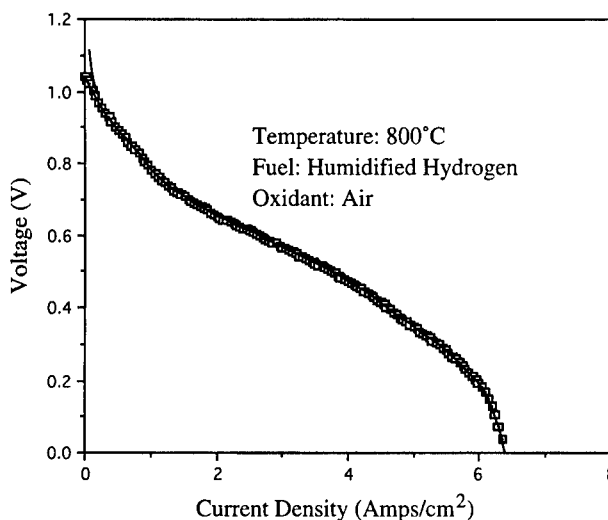
Fig. 5. The voltage, V, vs. current density, i, trace for an improved anode-supported cell tested at 800°C with humidified hydrogen as the fuel and air as the oxidant. The anode thickness was ~1.04 mm and the electrolyte (YSZ) thickness was ~10 μm. The symbols are the experimental data points while the curve is the best fit to Eq. (15). The parameters corresponding to the best fit are given in Table 1.

oxygen at the cathode/electrolyte interface is nearly zero), Amp/cm². The i_{as} and the i_{cs} can be given in terms of the respective electrode thicknesses, the respective effective binary diffusivities (which include the porosity and the tortuosity factors), and $p^o_{H_2}$ and $p^o_{O_2}$, respectively, where $p^o_{O_2}$ is the partial pressure of oxygen in the oxidant (0.21 atm for air as the oxidant) [6].

The data given in Fig. 2 are on some early cells wherein the porous YSZ layer for the prospective cathode was first deposited followed by the introduction of an aqueous salt solution of the cathode precursor. The microstructure in such cathodes was however rather coarse. Eq. (7) shows that the grain size of the YSZ in the cathode should be as small as possible. Thus, in later cells, a much finer cathode microstructure was developed. Also, in these cells, the YSZ electrolyte was typically about 10 μm in thickness; about half as thick as in cells for which the performance data are given in Fig. 2.

Fig. 5 shows a plot of V vs. i for an improved anode-supported cell tested at 800°C with humidified hydrogen as the fuel and air as the oxidant. The electrolyte thickness was about 10 μm and the anode thickness was about 1 mm. The corresponding power density vs. current density plot is shown in Fig. 6. As seen in Fig. 6, a power density as high as 1.9 Ω/cm²

was measured. Such a high power density was achieved by minimizing both activation and concentration polarizations through an optimization of the electrode microstructure. The symbols in Fig. 5 are the experimental data points and the curve is the best fit to Eq. (15). For an anode-supported cell, the
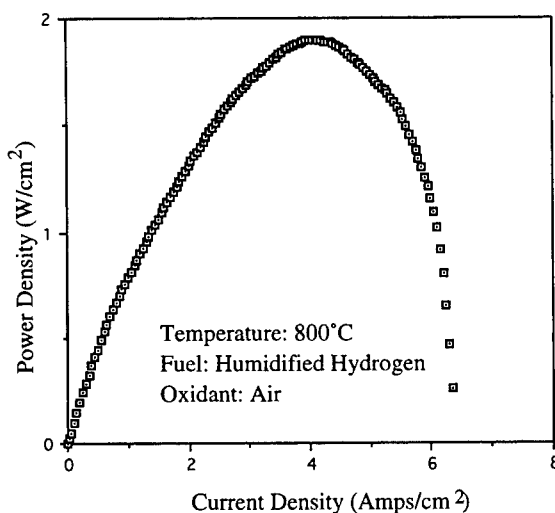

Fig. 6. The power density vs. current density, i, trace for the cell in Fig. 5. The maximum power density measured is ~1.9 Ω/cm².

anode thickness, l_a, is much greater than the cathode thickness, l_c, with the result that $i_{as} \ll i_{cs}$. Thus, the term containing i_{cs} from Eq. (15) can be neglected. Table 1 gives the parameters corresponding to the best fit to Eq. (15), as well as some of the experimentally measured parameters. The effective exchange current density, $i_{o(eff)}$, was estimated to be ~110 mA/cm^2, which is more than an order of magnitude higher than that corresponding to LSM on YSZ at 800°C. The electrolyte area specific resistance, R_i, from the best fit was estimated to be ~0.046 Ωcm^2. The electrolyte thickness was about 10 μm. With the resistivity of YSZ as ~50 Ωcm at 800°C, the estimated value of R_i is about ~0.05 Ωcm^2, in good agreement with the value obtained from the curve fit. Finally, the estimated value of the effective binary diffusivity on the anode side, $D_{a(eff)}$, is about 0.31 cm^2/s This value is reasonable when the porosity and the tortuosity factor are taken into account.

The theoretical analysis predicts that the initial concave-up curvature ($d^2V/di^2 \geq 0$) in V vs. i traces in anode-supported cells is due to two reasons [6]: (a) An activation polarization that is nonohmic (e.g. Tafel). (b) A concentration polarization that is

Table 1
Experimentally measured and curve-fitted parameters for the voltage vs. current density trace shown in Fig. 5

Parameter (description)	Parameter (symbol)	Measured	From the curve fit to the V vs. i
Anode thickness	l_a	1.04 mm	
Tafel coefficient	a		0.115
Tafel coefficient	b		0.0552
Effective exchange Current density	$i_{o(eff)}$		110 mA/cm^2
Cell area Specific Resistance (Ohmic)	R_i		0.046 Ωcm^2
Short circuit Current density	i_s	6.35 A/cm^2	
Anode limited Short circuit Current density	i_{as}		6.35 A/cm^2
Anode effective Binary diffusion Coefficient	$D_{a(eff)}$		0.31 cm^2/s
Maximum power Density		1.9 W/cm^2	

associated with too low a partial pressure of water vapor, embodied in the last term of Eq. (15). By contrast, any initial concave-up curvature ($d^2V/di^2 \geq 0$) in cathode-supported cells must entirely be due to a nonohmic activation polarization. The analytical form of the effect of concentration polarization in cathode-supported cells is such as to impart a convex-up curvature ($d^2V/di^2 \leq 0$) over the entire range of current densities [6]. Thus, if the activation polarization is ohmic, the curvature of V vs. i in cathode-supported cells must be convex-up ($d^2V/di^2 \leq 0$) over the entire range of current densities. Indeed, this has been observed in cathode-supported cells at 1000°C. In anode-supported cells, however, the initial curvature is expected to be concave-up ($d^2V/di^2 \geq 0$) even when the activation polarization is ohmic.

4. Summary

The present work has shown that the principal losses in SOFC are attributed to activation and concentration polarizations, especially when the electrolyte is a thin film supported on an electrode. Power densities as high as 1.9 Ω/cm^2 at 800°C were obtained with a thin film (~10 μm) of YSZ deposited on a relatively thick (1 mm), porous Ni + YSZ anode. The activation polarization on the cathode side can be substantially decreased by using a composite electrode comprising a mixture of an electrocatalyst, such as LSM, and an oxygen ion conductor, such as YSZ. The theoretical analysis predicts that activation polarization, as defined in terms of an effective charge transfer resistance, R_{ct}^{eff}, can decrease or increase with an increasing cathode thickness and attain a limiting value. For the set of parameters applicable to LSM as the electrocatalyst and YSZ as the oxygen ion conductor, the experimental results show that R_{ct}^{eff} decreases with an increase in the cathode thickness. Thus, a composite electrode of LSM + YSZ is very effective in lowering the activation polarization. It is known that activation polarization at the Ni + YSZ anode is generally much smaller than at the cathode. This suggests that R_{ct}^{eff} at the Ni + YSZ anode must be very small and that a composite electrode of Ni + YSZ is very effective in lowering the activation polarization at the anode. The

analysis of gas transport through a relatively thick anode shows that the V vs. i traces are expected to be nonlinear, in accord with the experimental results. Further, the analysis also shows that the initial concave-up curvature $(d^2V/di^2 \geq 0)$ in anode-supported cells has its origin in both activation as well as concentration polarizations. The present results show that the polarization effects in SOFC can be minimized through a microstructural optimization of the electrodes. As far as the activation polarization is concerned, the use of composite electrodes spreads the reaction zone from the electrolyte/electrode interface some distance into the electrode. In this sense, the electrolyte/electrode interface is a functionally diffuse interface.

Acknowledgements

References

[1] N.Q. Minh, J. Am. Ceram. Soc. 76 (1993) 563.

[2] N. Hisatome, K. Nagata, S. Kakigami, H. Omura, in: Fuel Cell Seminar Program and Abstracts, 1996 Fuel Cell Seminar, Orlando, FL, November 17–20, 1996, p. 194.

[3] Y. Miyake, M. Kadowaki, Y. Akiyama, T. Yasuo, S. Taniguchi, K. Nishio, in: Fuel Cell Seminar Program and Abstracts, 1996 Fuel Cell Seminar, Orlando, FL, November 17–20, 1996, p. 28.

[4] S.C. Singhal, in: Meeting Abstract of the Third International Symposium on Ionic and Mixed Conducting Ceramics, the 1997 Joint International Meeting, the Electrochemical Society and the International Society of Electrochemistry, Paris, France, August 31–September 5, 1997, p. 2498.

[5] H.P. Buchkremer, U. Diekmann, L.G.J. de Haart, H. Kabs, U. Stimming, D. Stover, in: 1996 Fuel Cell Seminar, sponsored by the Fuel Cell Organizing Committee, Washington DC, 1996, pp. 175–178.

[6] J.-W. Kim, A.V. Virkar, K.-Z. Fung, K. Mehta, S.C. Singhal, J. Electrochem. Soc. 146 (1) (1999) 69–78.

[7] T. Kenjo, S. Osawa, K. Fujikawa, J. Electrochem. Soc. 138 (1991) 349.

[8] T. Kenjo, M. Nishiya, Solid State Ionics 57 (1992) 295.

[9] H. Deng, M. Zhou, B. Abeles, Solid State Ionics 74 (1994) 75.

[10] T. Kenjo, Y. Yamakoshi, Bull. Chem. Soc. Jpn. 65 (1992) 995–1001.

[11] C.W. Tanner, K.-Z. Fung, A.V. Virkar, J. Electrochem. Soc. 144 (1) (1997) 21–30.

[12] E.A. Mason, A.P. Malinauskas, Gas Transport in Porous Media: The Dusty Gas Model, Elsevier, Amsterdam, 1983.

[13] R. Jackson, Transport in Porous Catalysts, Elsevier, Amsterdam, 1977.

[14] E.L. Cussler, Diffusion: Mass Transfer in Fluid Systems, Cambridge University Press, Cambridge, 1995.